THE JOURNAL OF PHYSICAL CHEMISTRY B

ARTICLE

pubs.acs.org/JPCB

Polyunsaturated and Saturated Phospholipids in Mixed Bilayers: A Study from the Molecular Scale to the Lateral Lipid Organization

C. Rosetti* and C. Pastorino

Departamento de Física, Centro Atómico Constituyentes CNEA, Av. Gral. Paz 1499, 1650 San Martín, Buenos Aires, Argentina
CONICET, Avda. Rivadavia 1917, C1033AAJ Cdad. de Buenos Aires, Buenos Aires, Argentina

ABSTRACT: Polyunsaturated lipids are remarkably flexible molecules, with a great influence on the membrane structure and dynamics, affecting from mechanical properties to domain segregation. In this work, we studied phospholipid mixtures of dipalmitoylphosphatidylcholine (DPPC) and diunsaturated phosphatidylcholine lipids (diunsPC) of different lengths, by means of molecular dynamic simulations of a coarse-grained interaction model. These diunsPC:DPPC binary mixtures show nonideal behavior characterized by one mixed phase with composition fluctuations on a length scale of nanometers. Motivated by this observation, we studied comprehensively the characteristics of molecular structure as a function of the compositional gradient. We analyzed orientational order profiles, density distributions, and pair−pair correlation functions between the molecule residues. We observed that, in diunsPC-enriched regions, DPPC tails become expanded and disordered, especially toward the membrane center. On the other hand, in the more condensed DPPC-enriched patches, diunsaturated acyl chains become displaced toward the interface instead of stretching along the membrane normal. From the comparison of the two diunsPC lipids of different tail length, we measured that the presence of a longer terminal saturated segment induces better mixing with DPPC, and most interestingly eliminates the up−down composition correlation measured with the shorter tail-diunsPC. At molecular level, there is a reduced redistribution of densities and changes in the local order as a function of composition. We interpret these results as indicative that the packing incompatibility between polyunsaturated and saturated lipids rules their mixing behavior.

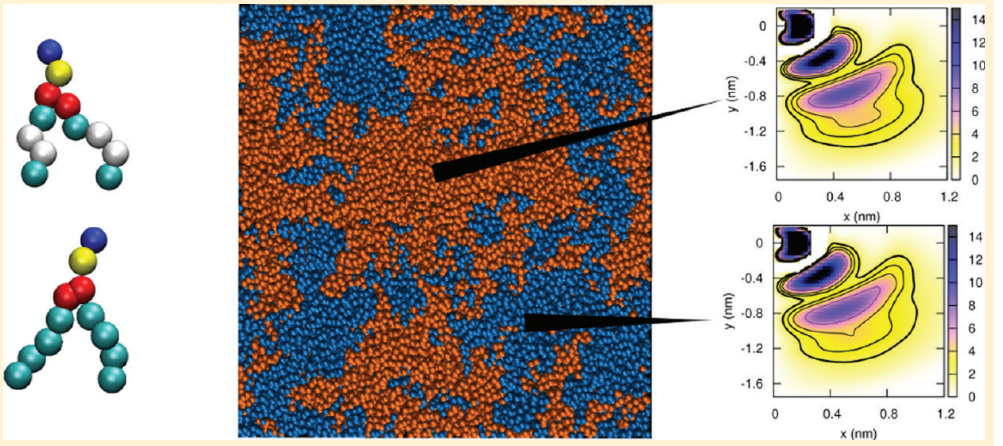

I. INTRODUCTION

Biological membranes have hundreds of different lipid species arranged in a dynamic structure. They present compositional asymmetries between leaflets and also on the lateral plane of the bilayer. The segregation of components resides on a less favorable interaction between different lipid types, and much of the lipid domains develop on a submicrometer scale.[1−3] Within the large compositional complexity of membranes, some species or groups of lipids were identified as key elements to give the membrane its material properties and structure. Among the phospholipids, one distinctive and relevant property is the degree of unsaturation, that goes from species completely bonded by saturated linkages, to others with multiple unsaturated bonds, up to a maximum of six per chain.[4] The double bond is a more rigid linkage that introduces a kink in the molecule, preventing a tight packing. On the other hand, alternated *cis* double bonds form extremely flexible chains due to the unusual conformational freedom of the carbons located in between the unsaturated linkages.[5] The rate of structural transitions, including the conversion to largely folded states, is highly increased compared to monounsaturated or saturated lipids. On average, the bent configurations bring the terminal portions of the tails closer to the interface.[5−9] In this sense, mixed chain phospholipids show an uneven distribution between the polyunsaturated fatty acid, which is shifted toward the aqueous interface, and the saturated chain, that becomes displaced toward the bilayer center.[7,10,11] The conformational and dynamic properties of polyunsaturated lipids can affect a wide range of material and dynamic properties of bilayers that include the loosening of chain packing,[5,10,12,13] increase of water permeability,[14] decrease of mechanical strength,[14] and reduction of bending stiffness and thickness.[13,15] Some other effects would be connected to the average shape of these lipids, such as an enhanced fusion rate and transition to nonlamellar phases, together with a

Received: August 31, 2010
Revised: November 24, 2010
Published: December 28, 2010

redistribution of the lateral tensions across the bilayer.[16−18] Moreover, it was postulated that the highly unsaturated species may also favor the lateral segregation in membranes.[4,19−23] Replacing a monounsaturated by a polyunsaturated phospholipid accentuates the phase segregation in ternary mixtures containing also cholesterol and a second phospholipid with saturated acyl chains.[20,23,24] In fact, liquid ordered−liquid disordered coexistence induces a drastic segregation of the saturated and polyunsaturated lipid components to one and the other separated phases. The main effect of the rigid and planar cholesterol molecule is an increase of acyl chain order and hydrophobic thickness, but the impact is weaker in the presence of polyunsaturated tails.[11,22,25] A number of experimental reports, corroborated by simulation results, have demonstrated a reduced affinity between cholesterol and polyunsaturated phospholipids which even leads to a significant relocation of cholesterol to the bilayer center and wobbling on a larger angle range.[11,22,25−28]

Molecular dynamics (MD) simulations of coarse grained models allow one to study phenomena on progressively larger time and length scales, by eliminating some set of degrees of freedom in the description of the system.[29−31] The Martini model, developed recently, is a coarse grain force field based on a 4-to-1 mapping of atoms to interaction sites, that proved to successfully reproduce a variety of structural and elastic properties of lipids.[32,33] This level of coarse graining preserves some chemical specificity, while it largely increases accessible time and spacial scales to microseconds and tens of nanometers, allowing the study of collective phenomena such as phase transitions or phospholipid mixing.[34,35] In this spirit, Marrink et al. were able to reproduce a realistic liquid ordered−liquid disordered phase coexistence in ternary mixtures of a coarse grain model of dipalmitoylphosphatidilcholine (DPPC), the diunsaturated dilinoleoylphosphatidylcholine (DLiPC), and cholesterol.[25]

Despite the interest on the role of polyunsaturation, there are relatively few studies on the properties of mixtures between phospholipids with different levels of unsaturation. Gel−fluid separation between DPPC and highly polyunsaturated phosphatidylcholines was found, with phase diagrams that show deviation from ideal behavior.[36,37] Incomplete demixing into nanometric domains was also found in binary phospholipid bilayers composed of sphingomyelin and a mixed chain *sn*1 saturated (16:0) *sn*2 polyunsaturated (22:6) phosphatidylethanolamine.[20,21,23]

In this paper, we studied equimolar binary mixtures of DPPC with diunsaturated phospholipids of different chain lengths. Taking advantage of the level of resolution of the Martini model, we focused on the coupling of changes at molecular scale to the compositional gradient on the nanometer range. We present first the surface mixing behavior of DPPC with diunsaturated phosphatidylcholine lipids. Next, we describe changes in the molecular structure that result from variations of the local composition. These two levels of organization are shown to be largely interrelated . The coexistence in the lateral plane involves significant molecular rearrangements as a function of the compositional gradient. The low affinity between both lipid types seems to stem from their different packing properties. We propose that this inherent incompatibility may be enhanced in the presence of cholesterol.

II. METHODS

A. Molecular Model and Simulation Details. We used the Martini coarse grained (CG) force field, version 2.0, developed by Marrink et al.,[32,33] to study mixtures and pure bilayers of symmetric

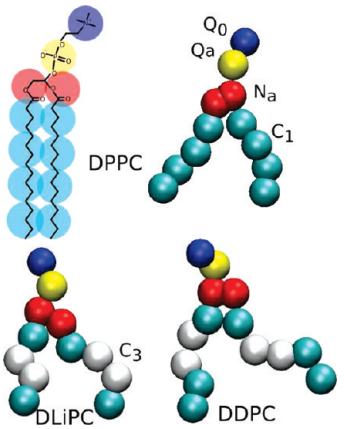

Figure 1. Saturated (DPPC) and diunsaturated (DLiPC and DDPC) coarse grain lipids used in this work, as given by the Martini model. Q, N, and C refer to bead types charged, nonpolar, and apolar. The subclass a reflects the capability of the phosphate and glycerol (glycerol + carbonyl) residues of being hydrogen bond acceptors, and the 0 indicates the inability of the trimethylammonium of participating in a hydrogen bond. The 1 to 5 categories discriminate inside a particle class, based on a hydrophilicity scale, from less to more polar; 1 is used for hydrophobic beads representing chain segments with saturated bonds, and 3 indicates the more hydrophilic character of the double bond. The lipid configurations were obtained from the simulations of pure bilayers. The cartoon representation of the DPPC molecule (upper left panel) illustrates the mapping of groups of atoms into interaction sites.

phospholipids having none or two unsaturations. The coarse graining consists of the mapping of about four heavy atoms into a single interaction site. Four types of beads are defined for lipids according to the level of hydrophilicity: charged Q, polar P, nonpolar N, and apolar C, used for the hydrophobic tails. Non-first-neighbor particles interact through a shifted Lennard-Jones potential, and the Coulomb interaction is represented by screened Coulomb potentials with a relative dielectric constant of $\varepsilon_{rel} = 15$, which takes the explicit screening of the Coulombic potential. The cutoff of the potentials is set to $R_c = 1.2$ nm for all the beads. The Coulomb potential is calculated only in the real space. All the lipids in this work, depicted in Figure 1, share the same topology for the headgroup, with two polar charged beads representing the negatively charged phosphate and positively charged trimethylammonium residues of phosphatidylcholine. Two nonpolar beads form the glycerol linkage, each representing the glycerol and carbonyl groups, and the lipid tails are four to five apolar (hydrophobic) beads long, each bead representing approximately four methylenes. The bending rigidity of the molecules is modeled by a harmonic bending potential of the form

$$V_b(\theta_{ijk}) = K_b(\cos(\theta_{ijk}) - \cos(\Theta_0))^2$$

where θ_{ijk} is the bond angle formed by three consecutive beads i, j, and k and Θ_0 is the equilibrium bond angle. These parameters are changed to introduce a single double bond from an equilibrium angle of $\Theta_0 = 180°$, and a bending elastic constant of $K_b = 25$ kJ/(mol·rad^2), used for saturated more straight tails, to $\Theta_0 = 120°$, and $K_b = 45$ kJ/(mol·rad^2). These changes introduce a kink in the molecule, which is matched with the bond angle distribution of atomistic simulations of unsaturated hydrocarbon chains.[33] The parametrization for the polyunsaturated lipids was taken from ref 28. The more flexible polyunsaturated chains are simulated by an even smaller bending equilibrium angle ($\Theta_0 = 100°$), and bending constant $K_b = 10$ kJ/(mol·rad^2), that reproduces the angle distribution

obtained by all-atom simulations with the GROMOS force field performed by Feller et al.[28] To mimic the increased polarizability of double bonds, the unsaturated CG beads are slightly more hydrophilic than the saturated counterparts . The saturated phospholipid with four tail beads is a coarse grained representation for DPPC as depicted in Figure 1. The topology of the diunsaturated phosphatidilcholine with a four-bead-long tail is an approximate model for the w6 dilinoleoyl PC, a 18:2 18:2 PC with two *cis* unsaturations at C9 and C12 (DLiPC). We also studied a diunsaturated phospholipid, which differs from DLiPC in an extra bead of type C1 added at the end of the chain. This would roughly represent the addition of a four-carbon saturated segment to the acyl chains. This lipid species will be referred to as DDPC throughout the paper. The parameters for this new bond were chosen to be the same as those of saturated DPPC (K_b = 45 kJ/(mol^{-1}·rad^{-2}) and Θ_0 = 180°). The MD simulations were performed with Gromacs package version 4.0.[38]

Two different bilayer sizes were simulated with explicit solvent, using a time step of 0.03 ps, updating the neighbor list every 10 steps, and saving 1 out of 1000 simulation steps. We prepared larger patches, with 1600 lipids, of pure membranes or equimolar mixtures of DPPC with a diunsaturated lipid. We simulated also smaller bilayers, with 400 lipids, of pure systems or mixtures that contained one single molecule of one of the components in a matrix of the second component. The bilayers were hydrated with 8 coarse grain water beads per lipid, equivalent to 32 real water molecules. All the simulations were performed at constant pressure and temperature. For pressure, the *xy* and *z* (lateral and normal) directions of the systems, were independently coupled to a Parrinello−Rahman barostat, at 1 bar in both directions, leading to a tensionless membrane. The parameters in the Gromacs implementation of the barostat were set at a coupling time constant of 2 ps and isothermal compressibility of $\chi = 3 \times 10^{-5}$ bar^{-1}. A weak coupling Berendsen algorithm[39] was independently applied on the lipids and water for maintaining the temperature at 300 K, with a relaxation time of 0.3 ps. The experimental transition temperature of DPPC is above this temperature, but the coarse grained DPPC melts at 295 K.[35] All the lipids used in the work are in the fluid phase at 300 K. The larger patches were simulated at least for 1.6×10^8 steps, which are roughly equivalent to 4.8 μs. This simulation time is an underestimation of the actual time sampled, because the dynamics of the coarse grained systems are accelerated with respect to the atomic detailed bilayers from 3 to 6 times, according to the authors of the CG model.[32] In applications of Martini's CG model, a standard factor of 4×, which compensates the speed-up of CG water, is usually reported to achieve a realistic time scale.[32,33] This mapping will be adopted here from now on, when indicating simulation times. The final 9.6 μs (8×10^7 steps) of the simulations were employed for data analysis. Molecular area and energy were used to check the equilibration of the membranes. For the equimolar mixtures, we also analyzed the average composition of the first lipid neighbors and the radial distribution function between both lipid components, which is dependent on the degree of mixing. The total time for equilibration is in the same order as the lipid diffusion across the simulation box length, which is a reasonable scale of time to attain good mixing. In the smaller patches, the measurements were made on single molecules, and to improve the statistical error, 48 μs trajectories were analyzed from simulations that ran 60 μs in total (5×10^8 MD time steps). In addition, we have checked that the analysis of a single lipid of the major component reproduces the average over all the lipids.

The equimolar mixtures were prepared from a pure patch of 1600 diunsaturated lipids, by changing randomly to DPPC the identity of half the molecules in each monolayer. The final configuration had an equal number of lipids in both leaflets. This state was taken as the starting point for the equilibration run of the 1:1 mixtures after minimizing the energy, with the steepest descent algorithm, to relax the angle bonds of both lipid types. A random binary mixture was also sampled by taking a single component membrane and randomly assigning the lipids to two different molecular identities.

B. Analysis. The thickness of membranes was calculated from the difference in the mean position of the phosphates in both leaflets. Each lipid molecule was assigned to the upper or lower monolayer according to the relative position in *z* direction of its phosphatidylcholine group center of mass, compared to the center of mass of its tails.

The mean molecular area was estimated as the area of the simulation box, $L_x \times L_y$, divided by the number of lipids per monolayer. This calculation does not take into account membrane undulations, which increase with the size of the patch. Nonetheless, no difference was observed between the smaller and larger bilayers. The bond orientational order parameter was calculated as the mean value of the second order Legendre polynomial of the bond angle:

$$P_2(\cos(\theta)) = \left\langle \frac{1}{2}(3\cos^2\theta - 1) \right\rangle$$

where θ is the angle between the vector connecting two consecutive beads and the direction $\hat{z}$, normal to the membrane. P_2 values are in the range $[-0.5,1]$, with the extreme cases corresponding to bonds completely perpendicular and parallel to the *z* direction, respectively. $P_2 = 0$ represents random orientation. This parameter was calculated averaging over each lipid bond, and also over 100 *z* slices along the membrane normal.

A pair−pair correlation function, $g(r,z)$, was calculated between the residues in each molecule and the center of mass of the glycerols. We selected this intramolecular reference because the glycerol location is rather indicative of the interface position. We used cylindric coordinates: the *z* position in the direction perpendicular to the membrane interface and a radial coordinate that lies on the *x*−*y* plane, tangent to the membrane. No information is lost with respect to a representation on *x*, *y*, and *z* directions, because the contours on each *z* slice are radially symmetric, as expected for lipids in the liquid phase. All values were normalized by the total number of beads.

A Voronoi tessellation analysis was performed on the trajectories using the *voro*$^{++}$ [40] program, configured for two dimensions. The Voronoi grid for each monolayer was separately computed by constructing the polygons that enclose the region of the space closest to the center of mass of each lipid. The analysis was used to calculate the average area available for each lipid and the composition of the lipids' first neighbors.

In the 1:1 mixtures, we compared the mixing behavior and analyzed possible coupling between molecular structural properties and the local composition. To this end, composition and average molecular parameters, such as $P_2(\cos(\theta))$, $g(r,z)$, and density profiles, were calculated on a grid for each configuration. Each lipid was assigned to a grid box according to the position of its center of mass. The analysis was performed dividing the sample box in grids from 3×3 until 12×12. This means a binning box length in the range of ~8 to 2 nm or a typical number of ~88 to 5 molecules/box. For such a small number of molecules, the instantaneous composition values will be discrete and will depend on the chosen binning. To standardize the analysis, the composition values, expressed as the molar fraction of DPPC, were discretized into four ranges of

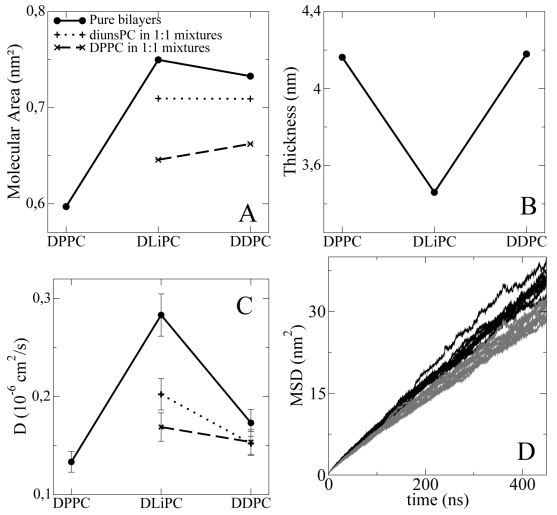

Figure 2. Mean molecular area (A), thickness (B), and diffusion coefficient (C) of DPPC and diunsPC lipids. The solid circles show the average values measured from pure bilayers. In parts A and C, the additional symbols depict the mean molecular area, calculated from Voronoi tessellation (A), and the diffusion coefficient (C), of DPPC (plus symbol) and the diunsPC (cross symbol) components in 1:1 DPPC:diunsPC mixed bilayer. Part D shows the mean square displacement curves for DPPC (gray lines) or DLiPC (black lines) in the equimolar DLiPC:DPPC membranes. The lines in parts A−C are to guide the eye. When not visible, the standard error bars are within the resolution of the symbols.

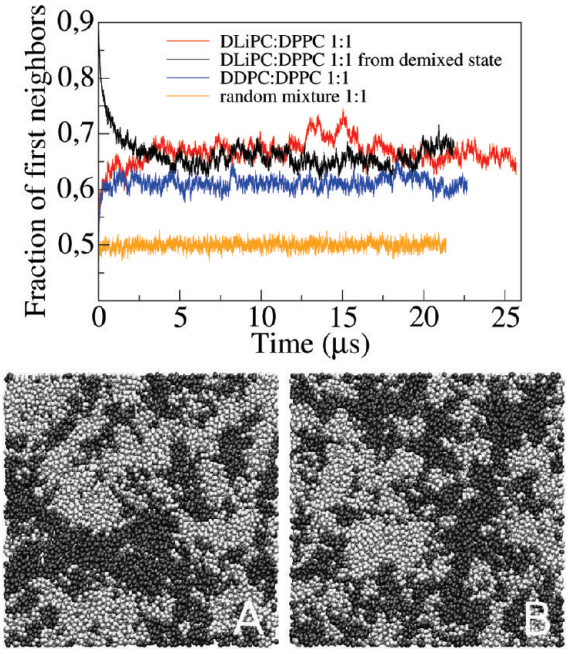

Figure 3. The top panel shows the fraction of DPPC neighbors to DPPC lipids as given by Voronoi tessellation, as a function of time. Images are snapshots of equimolar mixtures of DLiPC:DPPC (A) and DDPC:DPPC (B), with 1600 lipid molecules. DPPC is colored white and diunsPC dark gray. Water was removed for clarity.

0−0.25, 0.25−0.50, 0.50−0.75, and 0.75−1 and the pure compositions ($X_{DPPC} = 0$ and $X_{DPPC} = 1$) were saved separately. The results are typically shown for 10 × 10 grids, unless mentioned explicitly in the text.

The bead density profiles were calculated in the z direction, perpendicular to the membrane plane, dividing the MD box in 100 slices along the z coordinate. The errors were estimated by block averaging the total trajectories with a block size of 4×10^6 steps.

III. RESULTS

A. Structural and Dynamic Properties of the Pure DPPC and Diunsaturated Phosphatidilcholine Lipid Bilayers. We performed a first series of simulations with pure membranes to find a reference set of properties. The molecular area and thickness of membranes of the coarse grain lipids are shown in Figure 2, in panels A and B, respectively. The coarse graining of the model lipids necessarily neglects some chemical details, making possible only semiquantitative comparisons with experiments. In this sense, several trends are well reproduced by the molecular model as the increase in the mean molecular area for the polyunsaturated lipids (Figure 2A). This agrees with experimental data and all-atom simulation measurements made on mixed chain (*sn*1 saturated, *sn*2 unsaturated) phospholipids which found larger areas for progressively more unsaturated species.[4,5,13,41] It is also in line with results from pressure−area monolayer experiments on symmetric phospholipids.[41] Monolayer results show an expansion of 12 Å^2 for molecules with two extra *cis* double bonds (comparing di 18:2 PC to di 14:0 PC), in the order of the 14.4 Å^2 found in the coarse grained bilayers (Figure 2A). The increase of molecular area due to the presence of double bonds leads to a reduction of the hydrophobic thickness, so the acyl chains with one or more double bonds become shorter than saturated, or less unsaturated chains with the same carbon number.[10,15,42] The decrease in bilayer thickness from the coarse grained DPPC to DLiPC follows this trend. We also studied a diunsaturated lipid, DDPC, which has an additional bead at the end of the tails, with respect to DLiPC (see Figure 1). Pure bilayers of DDPC have a thickness similar to bilayers of DPPC (Figure 2). However, the packing area is similar to that of DLiPC bilayers. The DDPC molecule was studied with the purpose of isolating the effects of polyunsaturation from the thickness mismatch, and some interesting differences were observed from the comparison with DLiPC.

The diffusion coefficients describing the translational dynamics of the lipids are also shown in panel C of Figure 2. The values span over the range 0.1−0.3 cm^2/s, which are typical measurements for lipids in fluid membranes.[19] Reports on systematic determinations in a series of mixed chain phospholipids with one to six *cis* double bonds in *sn*2 show progressively faster lateral motion following the free area increase with the unsaturation level.[24] To the best of our knowledge, no data are available describing the behavior of diffusion in polyunsaturated phospholipids with symmetric chains. In the case of the coarse grain lipids, more than one competing factor is seemingly influencing the dynamics. Together with the increase of cross-sectional area from DPPC to DLiPC, there is a faster lipid diffusion.[43] On the other hand, the elongation of the hydrophobic chains from DLiPC to DDPC slows down the lipid motion. One possible factor contributing to the last effect is an increase in the contact surface between molecules.

B. Mixing Behavior of Diunsaturated Phosphatidylcholine:DPPC Equimolar Mixtures. Figure 3 shows illustrative snapshots of equimolar binary mixtures of DPPC with diunsaturated phosphatidylcholine lipids, from now on abbreviated diunsPC. The simulations show fluid phase membranes, with

nonideal mixing behavior without reaching macroscopic phase separation, both for DLiPC:DPPC mixtures, as already reported by Marrink et al.,[25] and also for 1:1 DDPC:DPPC. Compositional heterogeneities in the nanometric range (i.e., clusters rich in one type of lipid) are clearly observed to dynamically assemble and disassemble during the simulation. The deviation from ideal mixing may possibly indicate the proximity to a transition point to large scale segregation. We ran a control simulation starting from conditions closer to a fully demixed membrane to further check the stability of the mixed phase state. We observed that, beginning from a mosaic of four lipid patches containing 400 DPPC or DLiPC lipids each, the bilayer reaches the same final state as from an initially random-distributed configuration. For a more quantitative measure of the time evolution of the degree of mixing, we show the fraction of first neighbors of a lipid that are of its same type, along the simulation (Figure 3, top panel). We calculated this ratio over all the neighbors present in adjacent polygons in a Voronoi grid, traced from the position of the center of mass of each molecule. For 1:1 random distributed binary mixtures, the fraction of neighbor molecules of each kind fluctuates around 0.5 (see Figure 3). In 1:1 DDPC:DPPC and 1:1 DLiPC:DPPC, this fraction is larger and fluctuates around 0.61 and 0.67, respectively, indicating the formation of clusters, with comparatively larger segregation in DLiPC:DPPC bilayers.

The area and thickness differ less than 1% from the average values between the pure components in 1:1 DLiPC:DPPC bilayers. Instead, 1:1 mixtures of DDPC and DPPC show a nonlinear expansion of about 2 Å^2 in cross-sectional area and a decrease of thickness of around 0.1 nm (not shown). For each lipid component in the mixtures, we calculated the mean area available, using a 2D Voronoi tessellation, and the lateral diffusion (Figure 2A and C, stars for the DPPC and crosses for the diunsPC). Within the same mixed bilayer, diunsPC and DPPC components have a clearly different packing. Compared to their pure membranes, DPPC is more expanded and the diunsPC lipids are more tightly packed in the mixtures. We also found differences in the translational dynamics between DLiPC and DPPC mixed lipids. The difference is small but significant, as indicated by the non-overlapping mean square displacement curves shown in Figure 2D.

As a measure of the degree of mixing and the spatial order, we calculated the 2D radial pair−pair distribution function (RDF) between phosphate residues (see Figure 4A and B). In both diunsPC:DPPC mixtures, RDF curves are characteristic of fluid phase membranes with rapidly decaying order. Only the first two peaks of the distributions are clearly distinguished. As in the case of the average packing area and diffusion properties of each mixed lipid type, differences are also observed in the RDF results. A less structured organization surrounding the diunsPC component is noticed in comparison to DPPC. The RDF shows also that each lipid type is majorily surrounded by lipids of its same identity. In the case of DLiPC:DPPC mixtures, this enriched region extends up to $r \sim 6$ nm (approximately a quarter of the MD box length).

The distribution for the compositions was calculated for different length scales in each mixture. Composition values were measured on grids of different bin sizes in each leaflet separately. As an example, Figure 5C and D shows 2D representations of the composition measured on the snapshots shown in Figure 3, for 1:1 DLiPC:DPPC (Figure 5C) and 1:1 DDPC:DPPC (Figure 5D). This example analysis was performed on a 10 × 10 square grid which, for membrane patches of this size, has an average of eight lipid molecules per grid box and a bin length of ~2.3 nm. The average distributions are shown in Figure 5A and B. Composition values were quantified in a

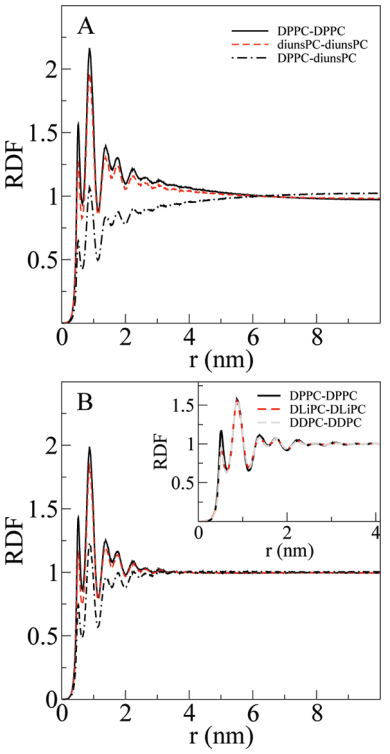

Figure 4. Two-dimensional radial pair−pair distribution function (RDF) for the phosphate beads in 1:1 DLiPC:DPPC (A) and DDPC:DPPC (B) bilayers, for DPPC−DPPC (solid black lines), diunsPC−diunsPC (dashed red lines), and diunsPC-DPPC (black point-dash line). The RDFs for the single component bilayers are shown in the inset.

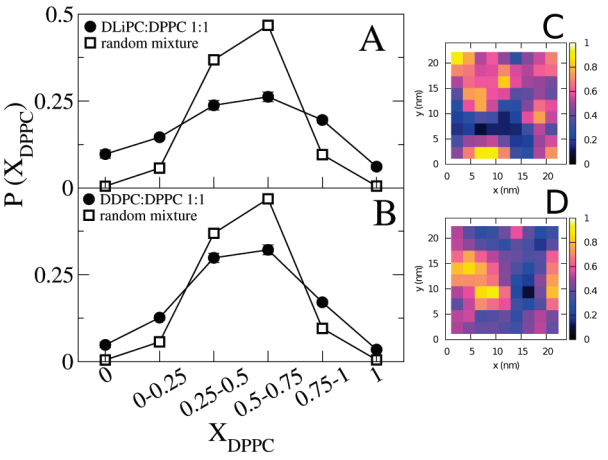

Figure 5. Probability distribution for the composition measured in a 10 × 10 grid (bin length 2.3 nm), on each membrane leaflet, for 1:1 DPPC:DLiPC (black circles in A), 1:1 DPPC:DDPC (black circles in B), or for a random mixture (open squares in A and B). The images on the right show the composition values on a color scale (white indicates pure DPPC and black pure diunsPC), calculated on the configurations represented in Figure 3. The error bars are within the resolution of the symbols and the lines are a guide to the eyes.

discrete scale of four DPPC mole fraction ranges (X_{DPPC}) of 0−0.25, 0.25−0.50, 0.50−0.75, and 0.75−1, and the pure compositions ($X_{DPPC} = 0$ and $X_{DPPC} = 1$) were analyzed as separate cases. An equimolar random mixture was also included as a reference (Figure 5, open squares). The asymmetry of the histograms is due to the fact

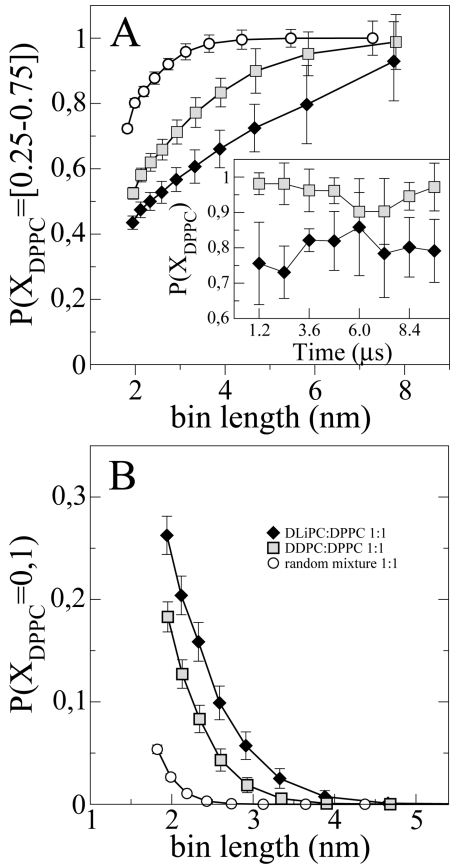

Figure 6. Probability distribution values of finding a composition in the range of $X_{DPPC} \in [0.25-0.75]$ (A), or pure patches ($X_{DPPC} = 0$ and $X_{DPPC} = 1$) (B), when the composition was analyzed in grids with different bin lengths. Black diamonds are for 1:1 DLiPC:DPPC, gray squares for 1:1 DDPC:DPPC mixtures, and white circles are for a random equimolar mixture (box simulation size = 477.6 nm^2). The inset in A shows the time evolution of the probability distribution of $X_{DPPC} \in [0.25-0.75]$ for a bin length of ~6.0 nm. Values were averaged over 1.2 μs intervals during the production run.

that the sampling is on a discrete and rather reduced set of composition values, because for this bin size there is only a small number of molecules per box. The distributions for 1:1 DLiPC:DPPC (Figure 5A) and 1:1 DDPC:DPPC (Figure 5B) are broader than those for the random case, indicating larger composition fluctuations, in the order of the bin length (~2.3 nm). To compare the spatial (in)homogeneity as a function of the length scale, we analyzed the distributions within the range of $X_{DPPC} \in [0.25-0.75]$ for different binnings (see Figure 6A). The results show that the composition varies on a larger length scale than for a random mixture, and DLiPC further increases the membrane inhomogeneity with respect to DDPC. The composition distribution remains stationary along the production run, as shown in the inset of Figure 6 for a box length of ~ 6nm. A similar analysis of the distribution on pure compositions (see Figure 6B) indicates that pure regions are detected up to a bin length of around ~3.3 nm for 1:1 DDPC:DPPC and slightly over ~3.8 nm for 1:1 DLiPC:DPPC bilayers (on average 17 and 22 molecules, respectively), while in the random mixtures single component regions are found only up to 2.5 nm (10 molecules).

We also analyzed the correlation of the composition between leaflets. Figure 7 shows the results obtained for a bin length of ~2.3 nm, in 1:1 DLiPC:DPPC (A) and 1:1 DDPC:DPPC (B)

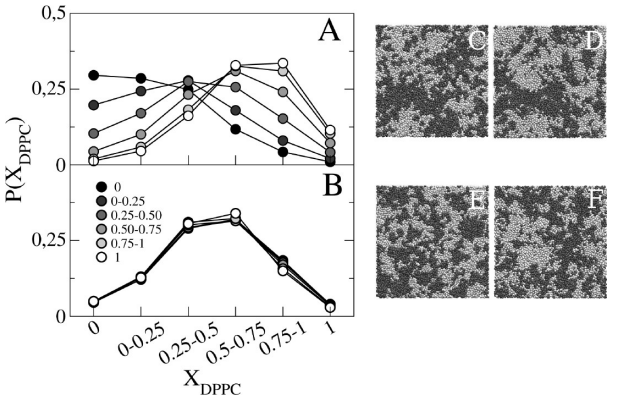

Figure 7. Probability distribution for the composition in one leaflet, given a certain composition in the apposed leaflet, in 1:1 DLiPC:DPPC (A) and 1:1 DDPC:DPPC (B) mixtures, for a bin size of ~2.4 nm. Symbols represent, from black to white, the distributions for increasing concentration of DPPC in the opposite monolayer (see the legend for a guide). Images are illustrative snapshots of the pattern in both leaflets for 1:1 DLiPC:DPPC (C and D) and 1:1 DDPC:DPPC (E and F), and correspond to the configurations shown in Figure 3.

mixtures. In the case of DDPC:DPPC mixtures, the compositions of both leaflets are independent, as the distributions are almost the same regardless of the composition in the opposite monolayer (Figure 7B). In DLiPC:DPPC membranes, instead, the composition in both layers tends to be coupled. Nevertheless, the distributions have a large amplitude, indicating that there are strong fluctuations in the up−down correlation (Figure 7A). In this sense, it is important to notice that this is not a correlation between stable segregated phases but coupled fluctuations between leaflets. It is interesting that the colocalization is more noticeable in regions of pure DLiPC than pure DPPC (Figure 7A). To highlight the result, we show images of both leaflets for each mixed bilayer on the right side of each composition distribution in Figure 7.

Along with the changes in composition, there are variations in the membrane dimensions. Figure 8 presents the thickness and mean cross-sectional area calculated from grid boxes with different compositions, in 1:1 diunsPC:DPPC mixtures. There are significant changes in the nanoscale range. 1:1 DLiPC:DPPC bilayers have progressively smaller molecular area and become vertically expanded as the local concentration of DPPC increases (see gray lines in Figure 8A and B). Meanwhile, in 1:1 DDPC:DPPC mixtures, there is also a contraction of the area in DPPC-rich patches, but in this case there is almost no thickness mismatch within the membrane (see Figure 8B). We have already described this behavior regarding the pure DPPC and DDPC bilayers. The difference in length between both molecules compensates the difference in equilibrium area, resulting in membranes of the same thickness. The regions with pure composition inside the mixtures resemble the pure bilayers, especially for diunsPC patches (circles and squares in Figure 8A and B). DPPC regions differ more from the pure bilayers, in that they are more expanded and thinner (triangles in Figure 8A and B). We show the results for different binnings. Some deviations in the area, especially for pure DPPC patches, are observed for small size boxes, but the area values converge for larger binnings. The curves shown well illustrate the variation range due to changes in the bin size. Variations in the sampling quality were likely introduced by density fluctuations. Nonetheless, these variations do not affect the trends described.

dx.doi.org/10.1021/jp1082888 |J. Phys. Chem. B 2011, 115, 1002–1013

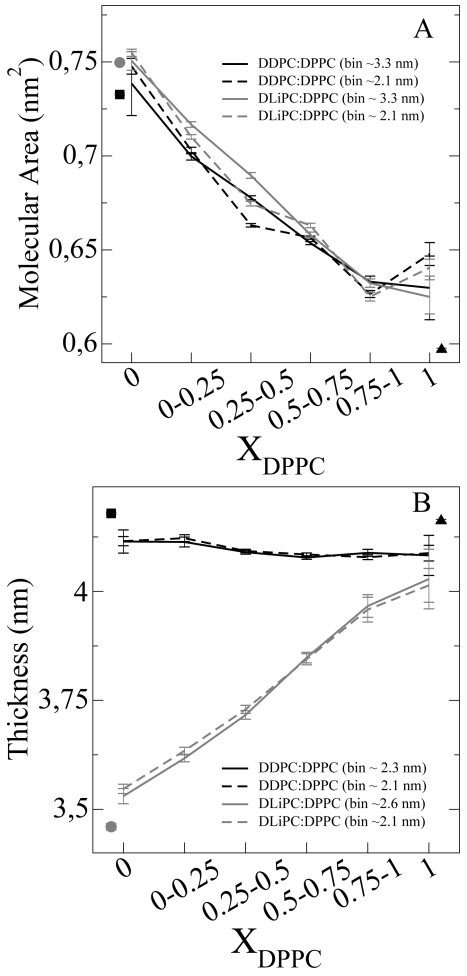

Figure 8. Mean molecular area (A) and thickness (B) calculated in grid boxes of different compositions. Samples of 1:1 DLiPC:DPPC are presented in gray lines and 1:1 DDPC:DPPC in black lines. Thickness was measured from the mean distance between the phosphate residues in grid boxes with the same composition in both leaflets. Mean molecular area was calculated from the average density of molecules per grid box. The symbols indicate the values for pure DLiPC (gray circles), DDPC (black squares), and DPPC (black triangles) membranes. We show the results for the minimum (dashed lines) and maximum (solid lines) bin sizes, that allowed the sampling of all compositions. The bin lengths are indicated in the legend.

C. Molecular Properties Dependent on the Molecular Environment. In sections C and D, we focus on describing the coupling of molecular structure to the composition of the environment. We analyzed changes through density distributions, pair−pair correlation functions between lipid residues, and orientational order parameter profiles. We present here the behavior of a single DPPC, or a diunsPC, mixed in a membrane of diunsPC or DPPC lipids, respectively. Pure bilayers and highly diluted lipids are valuable references to compare with changes associated with the compositional gradient in 1:1 mixtures (section D).

The packing, measured from a Voronoi tessellation, of a single DPPC or diunsPC molecule is largely modified to fit in a different host bilayer (Figure 9). The area available for DPPC is largely expanded to closely match that of the diunsPC lipid. In turn, diunsPC lipids become markedly condensed in a DPPC membrane.

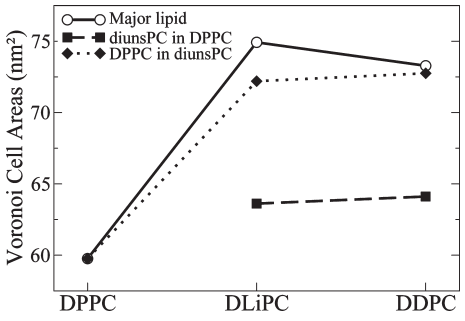

Figure 9. Mean area available per lipid, calculated from Voronoi tessellation, for a unique molecule of DPPC (black diamonds) or a diunsPC (black squares) mixed in a diunsPC or DPPC bilayer, respectively. The area of the lipids in pure membranes is also depicted (white circles). The error bars are within the resolution of the symbols. The lines are a guide to the eye.

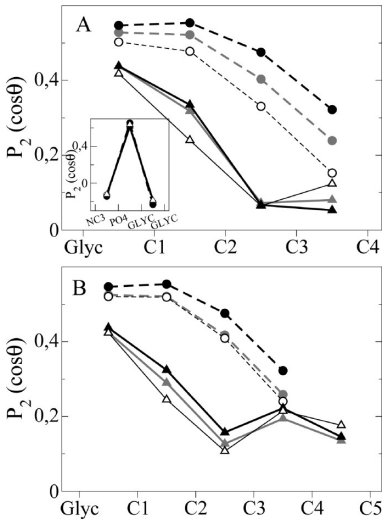

Figure 10. $P_2(\cos\theta)$ orientational order parameters for the bonds between the glycerol (Glyc) and tail beads (C1−C5) of DPPC (dashed lines, circles), and the diunsPC lipids (solid lines, triangles): DLiPC (A) and DDPC (B). Thin lines with white symbols correspond to a lipid molecule of DPPC or a diunsPC, mixed in a diunsPC or DPPC membrane, respectively. Thick lines with black symbols represent the lipid in its pure bilayer. The average values calculated from 1:1 diunsPC:DPPC mixtures are depicted with gray. The inset presents the headgroup bonds between the trimethylammonium (NC3), phosphate (PO4), and glycerol residues. The error bars are within the symbols.

Packing variations are usually associated with changes in the orientational order of the bonds. Figure 10 compares the orientational order profiles of DPPC (dashed lines) and the diunsPC (solid lines) in a pure membrane, with respect to the lipid as a single molecule mixed in a bilayer with a different degree of unsaturation (i.e., a diunsPC in a DPPC bilayer and DPPC in a diunsPC membrane). We show the tail bonds as the headgroup region presented mostly minor changes (see inset of Figure 10A). The flexible unsaturated bonds induce a steep decrease in the order parameter profile, in agreement with the results from all-atom MD simulations.[17] The orientational order of DPPC decreases along the tail when mixed in a diunsPC bilayer, in line with the larger lipid area, which usually permits more conformational disorder. For the diunsPC lipids mixed in DPPC, two different tendencies are observed: the orientational order increases toward the chain end but decreases closer to the

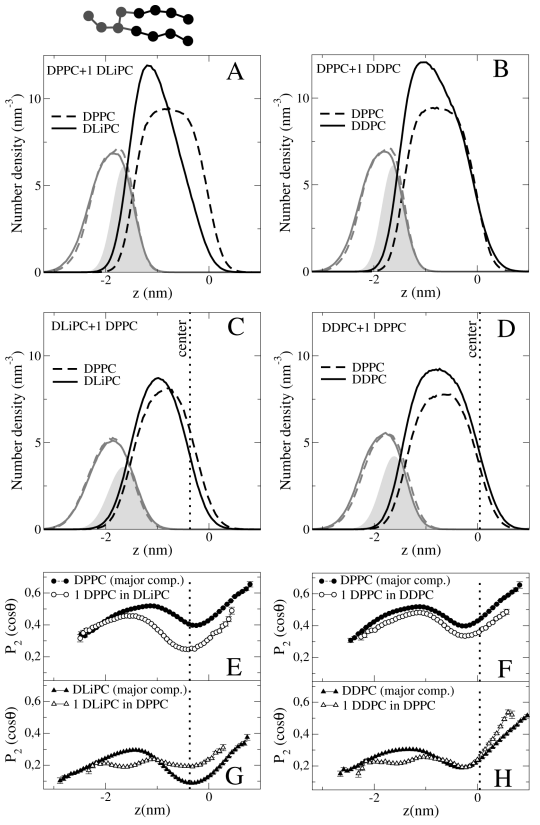

Figure 11. Density distributions (panels A−D) and orientational order parameter profiles (panels E−H), calculated along the membrane normal in one of the leaflets. DiunsPC lipids are represented by solid lines in panels A−D and triangles in panels G and H. DPPC is shown by dashed lines in panels A−D and circles in panels E and F. Panels A and B correspond to DPPC bilayers containing one DLiPC or one DDPC molecule respectively. Panels C and D show the results for a single DPPC lipid in a DLiPC or a DDPC membrane, respectively. In panels A−D, gray lines represent the headgroups, black lines the tails, and the gray area the average glycerol density. DiunsPC membrane profiles were shifted in z to match the glycerol maximum density with that of DPPC bilayers, shifting the bilayer center to the dotted line in panels C−H. Density values were rescaled to represent 200 molecules. In panels E−H, black symbols correspond to the lipid as the major membrane component and white symbols represent the lipid as one diluted molecule component. The cartoon of the lipid molecule at the top is given as a reference for the lipid orientation.

headgroup. This last result was not expected in view of the large reduction in the area per lipid (see Figure 9).

Further insight into the molecular rearrangements that were taking place was gained by comparing the density distributions (Figure 11A−D) and the orientational order parameter profiles (Figure 11E−H), for these systems along the membrane normal. The lipid density distributions in almost pure DLiPC and DDPC bilayers (see Figure 11C and D) show that the diunsPC tails are shifted toward the headgroup region, in comparison to DPPC. This behavior was also reported in highly curved DLiPC:DPPC vesicles[44] and is related to the large flexibility of polyunsaturated tails, that allows backbending of the chains toward the interface.[5] The observation is in good agreement with results from all-atom MD simulations, and experiments, showing that in mixed chain phospholipids the polyunsaturated tail is more closely associated with the interface than the saturated chain.[10,45,46]

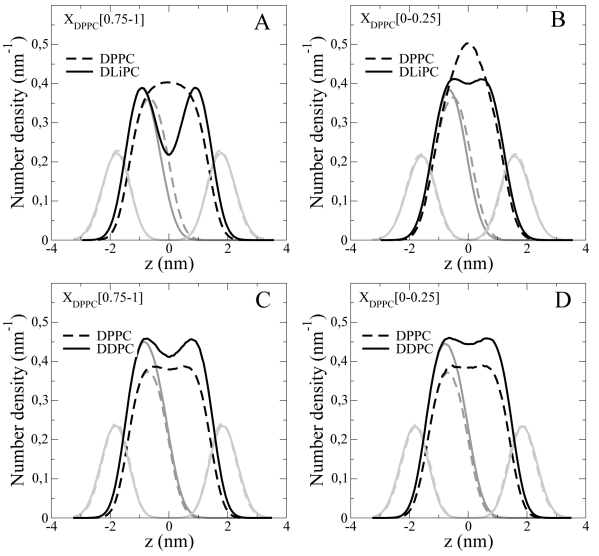

Figure 12. Density distribution of DPPC (dashed line) and of diunsPC lipids (solid line), along the membrane normal, in 1:1 DLiPC:DPPC (A, B) and 1:1 DDPC:DPPC (C, D) mixtures. Light gray lines represent the headgroups, and black lines represent the tails. Distributions were obtained from grid boxes with the same composition in both leaflets. The molar ratio of DPPC is $X_{DPPC} = [0.75-1]$ in parts A and C and $X_{DPPC} = [0-0.25]$ in parts B and D. All of the curves were rescaled to represent 100 lipids. Dark gray lines show the tail densities from one of the leaflets.

It is an interesting new result that the diunsPC lipids, when mixed in a DPPC membrane, acquire a highly asymmetric tail density distribution, with a large density increase toward the interface, and decreased overlap with DPPC chains (compare Figure 11A and B to Figure 11C and D). The orientational order parameter profiles further show that, accompanying the large density rearrangement, the orientational order decreases (compare black to white triangles in Figure 11G and H). Such a change reflects that the chain segments are, on average, more perpendicularly oriented to the membrane normal. The results are consistent with a net displacement of the tails from the interior of the membrane toward the interface. This results in a segregation along the z axis, indicating the low affinity between the lipids. The tails of a DPPC lipid mixed in a diunsPC membrane are rather symmetrically distributed with lower density values than in DPPC bilayers (compare Figure 11A and B to Figure 11C and D). DPPC tails become more disordered in a DLiPC environment, particularly toward the membrane center, where the DPPC/DLiPC relative density increases (see Figure 11E). A similar increase of disordered states was observed at the end of *sn*1-saturated chains esterified next to an *sn*2-polyunsaturated tail. The order profile was ascribed to the relative mass increase of the *sn*1-chain relative to the *sn*2-chain toward the membrane center.[10,42] In line with this interpretation, DDPC membranes, with a largely reduced lipid mismatch at the membrane center, induce only a small reduction in the "order" of DPPC tails (see Figure 11F), in spite of the increased lipid area (Figure 9).

D. Coupling of Molecular Structure to the Local Composition. We show in this section the correlation of changes in the molecular structure to the compositional gradient in 1:1 mixtures. The density distribution varies with DPPC mole fraction following the tendency previously described (see section C). Figure 12 shows that a local enrichment in DPPC leads to a density shift of the diunsPC tails from the membrane center toward the headgroup region, which decreases the overlap between DPPC and diunsPC tails. The effect is larger in

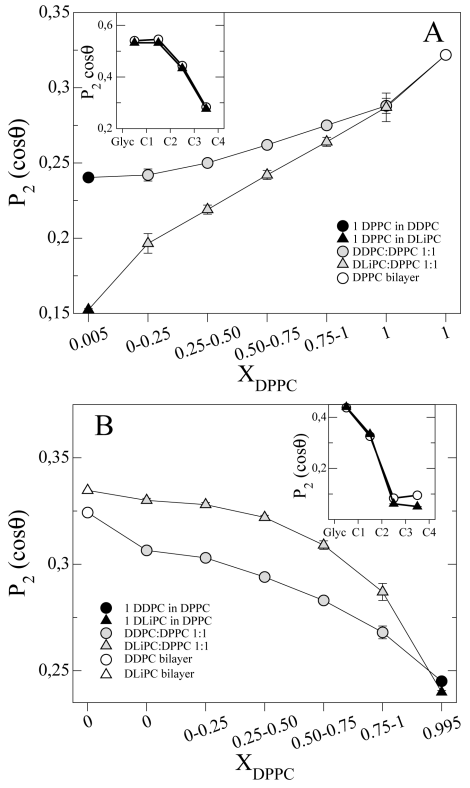

Figure 13. $P_2(\cos\theta)$ orientational order parameters for the last tail bond (C3−C4) in DPPC (A) and the C1−C2 bond in diunsPC lipids (B). White symbols correspond to pure bilayers. Black symbols represent a single DPPC or diunsPC molecule, mixed in a diunsPC or DPPC membrane, respectively. Gray symbols represent grid boxes with the indicated compositions, in 1:1 DLiPC:DPPC (triangles) or in 1:1 DDPC:DPPC (circles) mixtures. The vertical bars delimit the variation of the values due to changes in the bin length (from ∼2.0 to ∼3.3 nm). The insets show the orientational order parameters measured from grid boxes with pure DPPC (A) or pure DLiPC (B), in 1:1 DLiPC:DPPC mixtures. Black triangles are used for pure DLiPC, and white circles for pure DPPC, in the opposite leaflet. Lines are a guide for the eyes.

the mixtures with DLiPC (Figure 12A and B) than with DDPC (Figure 12C and D) . Density profiles also denote the bilayer thickening in DLiPC:DPPC and not in DDPC:DPPC, although in both mixtures the increase in DPPC induces the reduction of the mean molecular area (Figure 8A). The orientational order parameters also change with the local composition, as depicted in Figure 13. We follow the last bond of the DPPC tail (C3−C4 bond), that is more sensitive to the diunsPC environment, and the upper part of the tail (C1−C2 bond) of diunsPC lipids (see Figure 10 for a reference on the bond position in the molecule). Also in this case, the effect of the membrane environment follows the trend reported before (section C). We included, for comparison, the order parameter of pure bilayers (white symbols in Figure 13) and that of the lipid mixed as the unique molecule of its type (Figure 13, black symbols). In diunsPC lipids, the orientational order decreases with the concentration of DPPC, following a nonmonotonic trend: it becomes more sensitive at larger DPPC molar fractions (Figure 13B). Concomitantly, the tail in DPPC becomes progressively more ordered as its local concentration increases (Figure 13A). Whereas the effect of the composition is significant, when the orientational order parameters are averaged over the whole membrane, the impact of mixing can be small, particularly for diunsPC lipids (see Figure 10, gray lines). The local demixing, together with the nonlinear dependence on the composition (shown in Figure 13B), can hide some of the effects from the average measurements. Potentially associated with this, in DLiPC:DPPC bilayers with high curvature, Marrink et al. measured only subtle changes on the orientational order of DLiPC and DPPC due to mixing.[44] Interestingly, the curvature could also contribute to this difference.

We also found that the composition of the opposite leaflet can play a role in the orientational order of the lipids. Comparing grid boxes with pure composition, we observed that the final portion of DLiPC tails became more ordered for higher concentrations of DPPC in the apposed leaflet, as shown in the inset of Figure 13B. Such dependence was not observed for DPPC in DLiPC:DPPC mixtures (inset in Figure 13A), nor for any of the components in 1:1 DDPC:DPPC bilayers (not shown).

The redistribution of densities and changes in the orientational order suggest that variations in the mean shape of these lipids should be taking place depending on the local composition. The pair−pair correlation function of lipid residues $g_2(r,z)$, computed with respect to an intramolecular reference, gives an idea of the spatial distribution of the molecule. Figure 14 shows the $g_2(r,z)$ between the glycerols center of mass and the tails or glycerol residues in regions with different concentrations of DPPC. The $g_2(r,z)$ of DPPC shows more structure than that of DLiPC, in agreement with the higher configurational freedom of the chains and lower orientational order of DLiPC bonds. In fact, four regions with larger $g_2(r,z)$ values are clearly noticed in DPPC, matching the number of tail beads (Figure 14B and D). In DLiPC instead, tail residues have a higher overlap (Figure 14A and C). Significantly different lipid shapes are also evident. The diunsPC lipid is bulkier, shorter, and comparatively more extended in radial directions, toward the glycerol plane. The DLiPC and DPPC fit very well in the description proposed for polyunsaturated and saturated acyl chains of asymmetric lipids, in which they are assumed to adopt complementary density distributions.[7] Changes in the local composition are correlated to changes in the shape of the lipids, as can be observed by comparing Figure 14A and B with Figure 14C and D. To make these changes more evident, we defined the difference $g_{diff}(r,z) \equiv g_2(r,z;X_{DPPC}=[0.75-1]) - g_2(r,z;X_{DPPC}=[0-0.25])$, highlighting changes in $g_2(r,z)$ between regions of higher and lower concentrations of DPPC (see Figure 14E and F). The local increase of DPPC concentration induces DLiPC to acquire a wider wedge shape on the interface by shifting the mass from the membrane inside to a radially extended distribution near the glycerol plane. DPPC, in turn, becomes increasingly narrower toward the tail ends. $g_{diff}(r,z)$ is also shown for equimolar mixtures of DPPC and DDPC in panels G (DDPC) and H (DPPC) of Figure 14. The variations of $g_2(r,z)$ due to gradients in composition follow the same trend for DDPC:DPPC as for DPPC:DLiPC mixtures, although the changes are quite reduced in magnitude.

IV. DISCUSSION

Polyunsaturated lipids have a deep influence on membrane material and in-plane structural properties, playing an important role in domain segregation. This work presents a comprehensive MD simulation study of phospholipid mixtures of the fully saturated DPPC and diunsPC molecules of different chain lengths. We studied simultaneously the mixing behavior and changes in the molecular structure, showing an interesting interplay between the compositional gradient and lipid conformations, which involved significant redistribution of the lipid tails mass along the hydrophobic region.

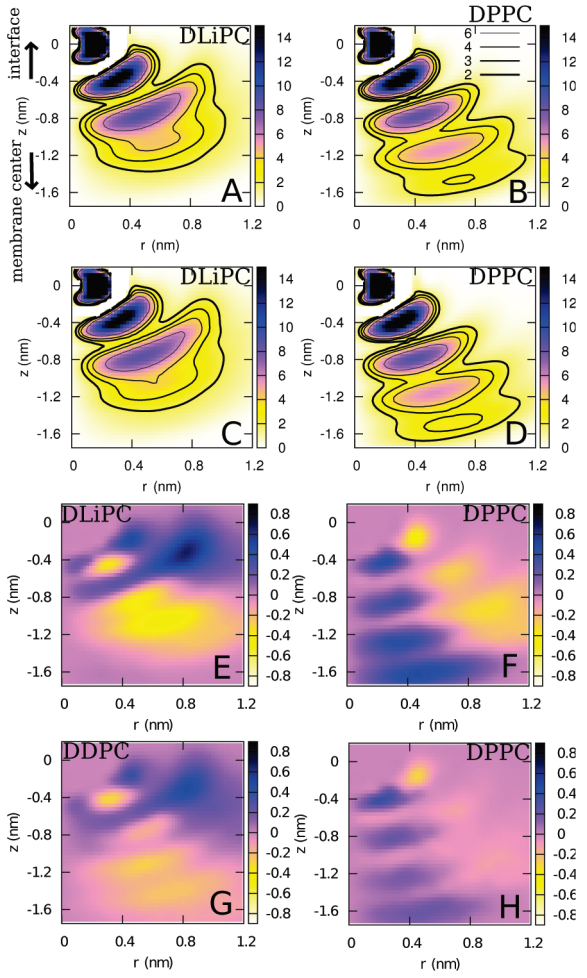

Figure 14. Pair−pair correlation functions in cylindric coordinates ($g_2(r,z) \times 10^3$) between the center of mass of the glycerol residues and the glycerol and tail beads of DLiPC (A and C) and DPPC (B and D) in 1:1 DLiPC:DPPC mixtures. The z coordinate is the position along the membrane normal, and the r coordinate is the radial distance from the normal. A and B correspond to molecules in grid boxes with $X_{DPPC} = [0-0.25]$. In parts C and D, the composition is $X_{DPPC} = [0.75-1]$. Parts E−H show $g_{diff}(r,z)$ (see the text for a definition), measuring the difference in $g_2(r,z)$ between regions with higher ($X_{DPPC} = [0.75-1]$) and lower ($X_{DPPC} = [0-0.25]$) DPPC concentrations in 1:1 DLiPC:DPPC (E and F) and 1:1 DDPC:DPPC (G and H). Parts E and G show the diunsPC lipids. Parts F and H represent the DPPC.

Equimolar diunsPC:DPPC phospholipid mixtures show nonideal behavior leading to one mixed phase with compositional fluctuations on the nanometer length scale. These compositional variations induce changes in membrane dimensions, mean cross-sectional area, and thickness, which in pure patches approach the values for pure membranes. This means a looser packing and, in the case of DLiPC, thinner hydrophobic regions, as the diunsPC concentration increases. Moreover, diunsPC components are surrounded by a less structured molecular arrangement than DPPC.

Our description on the molecular level is based on orientational order parameter profiles, density distributions, and pair−pair correlation functions, $g_2(r,z)$, between molecule residues. In these mixtures between symmetric lipids, we observed several features that matched the description of mixed chain polyunsaturated−saturated phospholipid bilayers.[5−11,45] One distinctive property is the inhomogeneous tail density distribution. Whereas diunsPC lipid chains are displaced toward the headgroup region, the relative density of DPPC saturated chains increases toward the membrane center. In line with this, diunsaturated chains show a more disordered orientation (lower orientational order parameters), with respect to saturated DPPC tails, that are, on average, more aligned to the membrane normal. The $g_2(r,z)$ of the diunsPC component shows less structure than that of DPPC, implying a larger overlap between tail residue distributions. It also denotes a bulkier shape of the acyl chains, compared to the more stretched DPPC. The emerging description is a complementary distribution of densities and mean shapes between the diunsPC and DPPC components at the hydrophobic region.

Analyzing differences in the tail density distributions, in relation to the compositional gradient, gives some insight into the interaction between lipid types. As the local concentration of the diunsPC component increases, the lipid packing resembles more the conformation in pure diunsPC membranes. In DPPC tails, the looser packing results in a progressive decrease in the orientational order, especially toward the tail end, and the acyl chains span over a wider volume. Although the general trend is the same, we observed some differences between DDPC:DPPC and DLiPC:DPPC mixtures which are discussed below. On the other hand, in regions with increased concentration of DPPC, where the local membrane properties resemble more pure DPPC bilayers, diunsPC tails become displaced toward the glycerols, and extend on the interface plane, segregating from the saturated tails. The decrease in the order parameters, and changes in $g_2(r,z)$, also sense this rearrangement. The results indicate a low affinity between the lipids, as diunsPC chains move toward a more interfacial location instead of extending along the membrane normal and maximizing closer tail−tail lipid contacts. The behavior possibly evidences the tendency of polyunsaturated chains to avoid stretching, adopting a different conformational solution to a tighter packing. Moreover, the slightly hydrophilic character of the double bonds would likely favor a more proximate contact to the hydrocarbon−water interface. The effect is observed in both diunsaturated lipids, DLiPC and DDPC, which differ in the saturated terminal region of the tail. The behavior is reminiscent of conformational changes, measured as a function of dehydration, in a mixed chain saturated−polyunsaturated phospholipid (i.e., 18:0 22:6 PC).[47,48] In this case, the removal of water leads to a progressive condensation of the fluid membrane until a transition to a different liquid lamellar phase occurs. This transition takes place with lateral expansion of the area, and a decrease in chain order parameters.[47,48] In our simulations, we also observed those changes (i.e., the decrease of the order and radial expansion of the polyunsaturated lipids) in the DPPC-rich, denser patches. This may represent a more general response of polyunsaturated acyl chains to certain packing restrictions. It would be interesting to contrast our simulation results with experimental measurements on mixtures with saturated lipids.

The addition of a longer saturated segment at the end of the tails, from DLiPC to DDPC, virtually eliminates the thickness mismatch but maintains the difference in the cross-sectional area, with respect to DPPC. This modification induces better mixing with DPPC and, at the same time, weakens the effect of the composition on the measured molecular rearrangements. In this sense, the orientational order of DPPC tails, and of the final portion of DDPC chains, is only slightly affected by compositional changes in DDPC:DPPC mixtures. Moreover, the shape of the tails, as given by $g_2(r,z)$, is also less dependent on the composition. The same is observed for the redistribution of tail

densities along the membrane normal, in comparison to DLiPC:DPPC mixed bilayers. One possible factor contributing to the better mixing is the decrease of hydrophobic length mismatch, that can favor demixing between lipids.[49] On the other hand, the interaction between DPPC and the terminal region in DDPC, with packing tendencies similar to saturated acyl chains, may partially compensate for the steric repulsion at the upper tail region. Interestingly, similar results were obtained from the comparison between mixed chain saturated−polyunsaturated phospholipids that differed in one double bond at the tail end.[46] A more homogeneous density distribution of the chains and less decrease in the orientational order of the saturated chain were observed after the loss of one double bond.[46] The authors proposed that the longer final saturated segment would likely extend toward the bilayer midplane, eventually limiting the upward displacement of the apical tail region.

When replacing DLiPC for DDPC, we found that the correlation between the composition fluctuations in both leaflets was no longer observed. Although further study is needed to understand this difference, the greatest similarity between the tail end of DPPC and DDPC will likely reduce the tension in the bilayer midplane. Probably related to this, we observed changes in the orientational order of the DLiPC tail end, induced by the opposite leaflet composition, in DLiPC:DPPC bilayers. On the contrary, we did not measure changes in DDPC or DPPC in DDPC:DPPC mixtures.

We observed that the local demixing relieves the large packing differences between the saturated and polyunsaturated mixed lipids. These are shown otherwise in the redistribution of densities and changes in the molecule shapes as a function of changes in the local composition. The results may be relevant to the segregation triggered by cholesterol, which may enhance this inherent packing incompatibility. The more rigid and densely packed liquid ordered phase will likely hinder the mixing of the polyunsaturated lipids, in agreement with Lindblom et al.[19] It would also decrease the relative affinity of the saturated lipid for the loosely packed polyunsaturated-rich phase, in line with the proposal in Kurcerka et al.[27] In this line, it is interesting to note that, in a DPPC-rich environment, the order of polyunsaturated tails is only slightly affected (i.e., the decrease in the first part of the tail is counterbalanced by the increase at the chain end). In the liquid ordered phase, however, the orientational order of DLiPC chains is reported to increase on average.[25]

Further work is being carried out to compare the present results with mixtures of saturated and monounsaturated phospholipids, and also with asymmetric phospholipids, with one polyunsaturated and one saturated chain. In the last case, the intramolecular packing tensions are expected to have an impact on the lateral composition.

AUTHOR INFORMATION

Corresponding Author

*E-mail: rosetti@tandar.cnea.gov.ar.

ACKNOWLEDGMENT

We thank Z. Gamba for useful discussions on the subject and the kindness of reading the manuscript. CONICET is gratefully acknowledged for the financial support (PIP 2008 No. 112-200801-00403). We thank also CNEA for support and computer power through the BAPIN 177 2010 and MINCYT (PICT 2005 No. 32198).

REFERENCES

(1) Edidin, M. *Trends Cell Biol.* **2001,** *11,* 492.
(2) Honerkamp-Smith, A. R.; Cicuta, P.; Collins, M. D.; Veatch, S. L.; den Nijs, M.; Schick, M.; Keller, S. L. *Biophys. J.* **2008,** *95,* 236.
(3) Rosetti, C. M.; Maggio, B. *Biophys. J.* **2007,** *93,* 4254.
(4) Stillwell, W.; Wassall, S. R. *Chem. Phys. Lipids* **2003,** *126,* 1.
(5) Feller, S. E.; Gawrisch, K.; MacKerell, A. D., Jr. *J. Am. Chem. Soc.* **2001,** *124,* 318.
(6) Saiz, L.; Klein, M. L. *Biophys. J.* **2001,** *81,* 204.
(7) Eldho, N. V.; Feller, S. E.; Tristam-Nagle, S.; Polozov, I. V.; Gawrisch, K. *J. Am. Chem. Soc.* **2003,** *125,* 6409.
(8) Huber, T.; Rajamoorthi, K.; Kurze, V. F.; Beyer, K.; Brown, M. F. *J. Am. Chem. Soc.* **2001,** *124,* 298.
(9) Feller, S. E. *Chem. Phys. Lipids* **2008,** *153,* 76.
(10) Rajamoorthi, K.; Petrache, H. I.; McIntosh, T. J.; Brown, M. F. *J. Am. Chem. Soc.* **2004,** *2004,* 127.
(11) Pitman, M. C.; Suits, F.; MacKerell, A. D.; Feller, S. E. *Biochemistry* **2004,** *43,* 15318.
(12) Mitchell, D. C.; Litman, B. J. *Biophys. J.* **1998,** *74,* 879.
(13) Koening, B. W.; Strey, H. H.; Gawrisch, K. *Biophys. J.* **1997,** *73,* 1954.
(14) Olbrich, K. C.; Rawicz, W.; Evans, D. E. *Biophys. J.* **2000,** *79,* 321.
(15) Rawicz, W.; Olbrich, K. C.; McIntosh, T; Evans, D. E. *Biophys. J.* **2000,** *79,* 328.
(16) Cantor, R. S. *Chem. Phys. Lipids* **1999,** *101,* 45.
(17) Ollila, S.; Hyvonen, M. T.; Vattulainen, I. *J. Phys. Chem. B* **2007,** *111,* 3139.
(18) Shaikh, S. R.; Brzustowicz, M. R.; Stillwell, W.; Wassall, S. R. *Biochem. Biophys. Res. Commun.* **2001,** *286,* 758.
(19) Lindblom, G.; Orädd, G. *Biochim. Biophys. Acta* **2009,** *1788,* 234.
(20) Shaikh, S. R.; Dumaual, A. C.; Catillo, A.; LoCascio, D.; Siddiqui, R. A.; Stillwell, W.; Wassall, S. R. *Biophys. J.* **2004,** *87,* 1752.
(21) Shaikh, S. R.; Brzustowicz, M. R.; Gustafson, N.; Stillwell, W.; Wassall, S. R. *Biochemistry* **2002,** *41,* 10593.
(22) Huster, D.; Arnold, K.; Gawrisch, K. *Biochemistry* **1998,** *37,* 17299.
(23) Soni, S. P.; LoCascio, D.; Liu, Y.; Williams, J. A.; Bittman, R.; Stillwell, W.; Wassall, S. R. *Biophys. J.* **2008,** *95,* 203.
(24) Filippov, A.; Orädd, G.; Lindblom, G. *Biophys. J.* **2007,** *93,* 3182.
(25) Risselada, H. J.; Marrink, S. J. *Proc. Natl. Acad. Sci. U.S.A.* **2008,** *105,* 17367.
(26) Harroun, T. A.; Katsaras, J.; Wassall, S. R. *Biochemistry* **2006,** *45,* 1227.
(27) Kurcerka, N.; Marquardt, D.; Harroun, T. A.; Nieh, M.-P.; Wassall, S. R.; de Jong, D. H.; Schafer, L. V.; Marrink, S. J.; Katsaras, J. *Biochemistry* **2010,** *49,* 7485.
(28) Marrink, S. J.; de Vries, A. H.; Harroun, T. A.; Katsaras, J; Wassall, S. *J. Am. Chem. Soc.* **2008,** *130,* 130.
(29) Venturoli, M.; Sperotto, M. M.; Kranenburg, M.; Smit, B. *Phys. Rep.* **2006,** *437,* 1.
(30) Müller, M.; Katsov, K.; Schick, M. *Phys. Rep.* **2006,** *434,* 113.
(31) Pastorino, C.; Binder, K.; Müller, M. *Macromolecules* **2009,** *42,* 401.
(32) Marrink, S. J.; de Vries, A. H.; Mark, A. E. *J. Phys. Chem. B* **2004,** *108,* 750.
(33) Marrink, S. J.; Risselada, H. J.; Ye_mov, S.; Tieleman, D. P.; de Vries, A. H. *J. Phys. Chem. B* **2007,** *111,* 7812.
(34) Faller, R.; Marrink, S. J. *Langmuir* **2004,** *20,* 7686.
(35) Marrink, S. J.; Risselada, J.; Mark, A. E. *Chem. Phys. Lipids* **2005,** *135,* 223.
(36) Stillwell, W.; Jenski, L. J.; Zerouga, M.; Dumaual, A. C. *Chem. Phys. Lipids* **2000,** *104,* 113.
(37) Dumaual, A. C.; Jenski, L. J.; Stillwell, W. *Biochem. Biophys. Acta* **2000,** *1463,* 395.

(38) van der Spoel, D.; Lindahl, E.; Hess, B.; Groenhof, G.; Mark, A. E.; Berendsen, H. J. C. *J. Comput. Chem.* **2005,** *26*, 1701.
(39) Berendsen, H. J. C.; Postma, J. P. M.; Van Gunsteren, W. F.; Dinola, A.; Haak, J. R. *J. Chem. Phys.* **1984,** *81*, 3684.
(40) Rycroft, C. H.; Grest, G. S.; Landry, J. W.; Bazant, M. Z. *Phys. Rev. E* **2006,** *74*, No. 021306 (URL: http://math.lbl.gov/voro++).
(41) Smaby, J. M.; Momsen, M. M.; Brockman, H. L.; Brown, R. E. *Biophys. J.* **1997,** *73*, 1492.
(42) Petrache, H. I.; Salmon, A.; Brown, M. F. *J. Am. Chem. Soc.* **2001,** *123*, 12611.
(43) Almeida, P. F.; Paulo, F. F.; Vaz, W. L. C.; Thompson, T. E *Biochemistry* **1992,** *31*, 6739.
(44) Risselada, H. J.; Marrink, S. J. *Phys. Chem. Chem. Phys.* **2009,** *11*, 2056.
(45) Everts, S.; Davis, J. H. *Biophys. J.* **2000,** *79*, 885.
(46) Eldho, N. V.; Feller, S. E.; Tristam-Nagle, S.; Gawrisch, I. K *J. Am. Chem. Soc.* **2003,** *125*, 6409.
(47) Binder, H.; Gawrisch, K. *Biophys. J.* **2001,** *81*, 969.
(48) Binder, H.; Gawrisch, K. *J. Phys. Chem. B* **2001,** *105*, 12378.
(49) Risbo, J.; Sperotto, M. M.; Mouritsen, O. G. *J. Chem. Phys.* **1995,** *103*, 3643.